Modeling analysis and optimization of a multi-wafer reactor for GaN HVPE

Quasi-thermodynamic model of GaN HVPE

The model is based on the quasi-thermodynamic description of surface kinetics [1] and detailed macroscopic description of species, mass, momentum, heat, and radiation transfer. The quasi-thermodynamic model of surface kinetics assumes that adsorption and desorption represent the limiting stages of surface processes while the other stages proceed under the quasi-equilibrium conditions. This idea allows avoiding a detailed description of the poorly known surface kinetic mechanism in III-nitride HVPE and to reach good agreement of the computed and experimental data using a few kinetic parameters. The essential gaseous reactive species to be accounted for has been selected using the mass-spectrometric data [2] and results of thermodynamic analysis [3]. The model has been carefully verified by comparison of the computed and experimental data on the crystal growth rate as a function of process parameters. An example of such verification is shown in Fig.1 where the computed dependence of the growth rate on temperature in the atmosphere of He or H_2 is compared with the data of Seifert et al [4]. Good agreement of the computed and experimental data in a wide temperature range is seen.

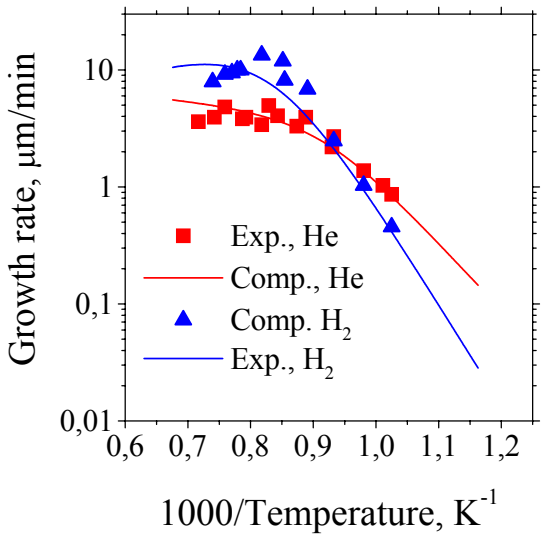

Figure 1. *Computed dependencies of the GaN growth rate on temperature in the atmosphere of He or H_2 in comparison with the data of Seifert et al [4].*

Using this model, we have performed altogether the works as follows:

- Analysis of the published data on the design of single-wafer reactors for III-nitride HVPE and selection of most prospective reactors;
- Simulation and optimization of the selected single-wafer reactors;
- Design of multi-wafer reactors based on scaling of the selected single-wafer reactors;
- Simulations of the scaling-based multi-wafer reactors;
- Original modification of the multi-wafer reactor design, simulations and preliminary optimization of the modified multi-wafer reactors;
- Final optimization of the modified multi-wafer reactors;
- Analysis of transitional effects in change of the species supply in the optimized reactors.

Some selected results of these works are presented below.

Single-wafer reactors

Analysis of the literature data has shown that vertically designed reactors suggest some advantages in III-nitride HVPE, providing better epilayer uniformity and lower reactor contamination with the parasitic deposits. Then, with focus on the vertical reactor design, we have selected two most prospective reactors for further analysis, they are an axially symmetric reactor with the species supply through a set of coaxial annular inlets [5] and a tube reactor with the species supply through a set of separate parallel tubes [6].

Careful simulations and optimization has shown that the former case provides much better growth characteristic, for which reason we consider here only this reactor. Some results of simulations and optimization of III-nitride HVPE in such reactor are shown in Figs. 2, 3. Here, the 52 mm diameter susceptor (the other reactor sizes can be derived from the figure by direct scaling) rotates at a rate of 60 rpm, 0.04 slm GaCl + 1.4 slm Ar are supplied through the central tube, 3 slm Ar - through the middle annular channel, and 1.2 slm NH_3 + 0.25 slm Ar - through the external annular channel. Fig. 2a shows the resulting flow pattern in the whole reactor and near the susceptor on a larger scale. A mighty vortex is seen to be generated above the susceptor in the conic part of the reactor. In this case, the vortex is largely produced by the mighty stream of GaCl + Ar coming into the reactor through the central injector. A distinct velocity boundary layer is also observed above the susceptor. Figs. 2 b and c display the computed uniform temperature distribution and non-uniform V/III ratio distribution in the reactor.

An example of the reactor optimization is given in Fig.3. Here, the radial distributions of the growth rate and V/III ratio are presented in variation of the characteristic reactor sizes as follows:

- All species injectors are 3 mm lower (line 2);
- All species injectors are 6 mm lower (line 3);
- All species injectors are 9 mm higher (line 4);
- Ar injector is 6 mm smaller in diameter (line 5);
- GaCl injector is 4 mm larger in diameter (line 6).

Smoothing of the central maximum in the growth rate distribution in elevation of the injectors (see lines 1-4) confirms the fact that the growth rate non-uniformity is largely related to the effect of central gas stream. This stream compresses the concentration boundary layer at the central part of the susceptor and thereby increases the species fluxes and crystal growth rate. Cases 4 and 5 are seen to give the desired average growth rate (5-15 μm/hr) but do not provide sufficiently high uniformity of its radial distributions (standard deviation form the average value is desired to be lower than 10%).

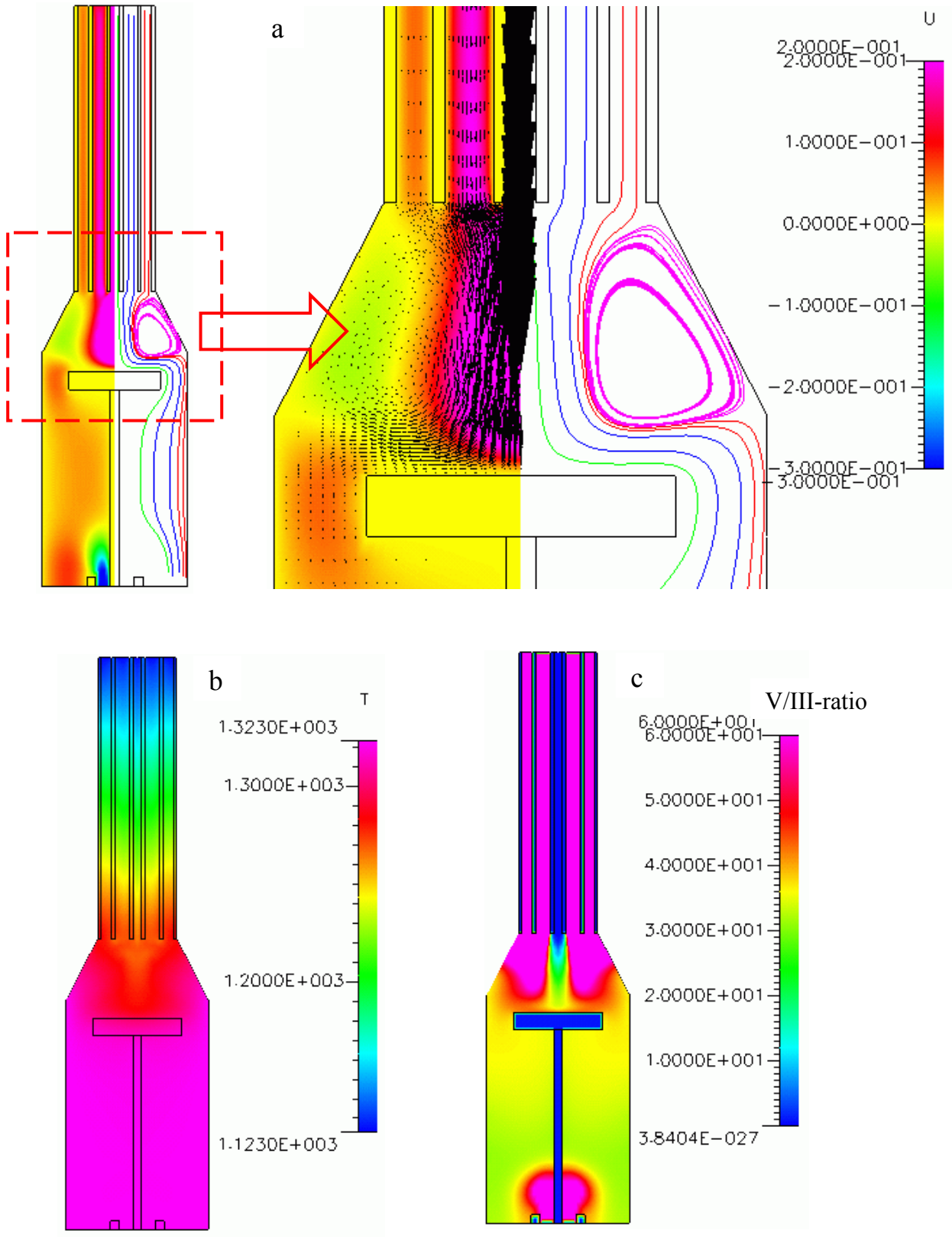

Figure 2. *Flow pattern (a) and distributions of temperature (b) and V/III ratio (c) in the axially symmetric vertical single-wafer reactor with the species supply through a set of coaxial annular inlets.*

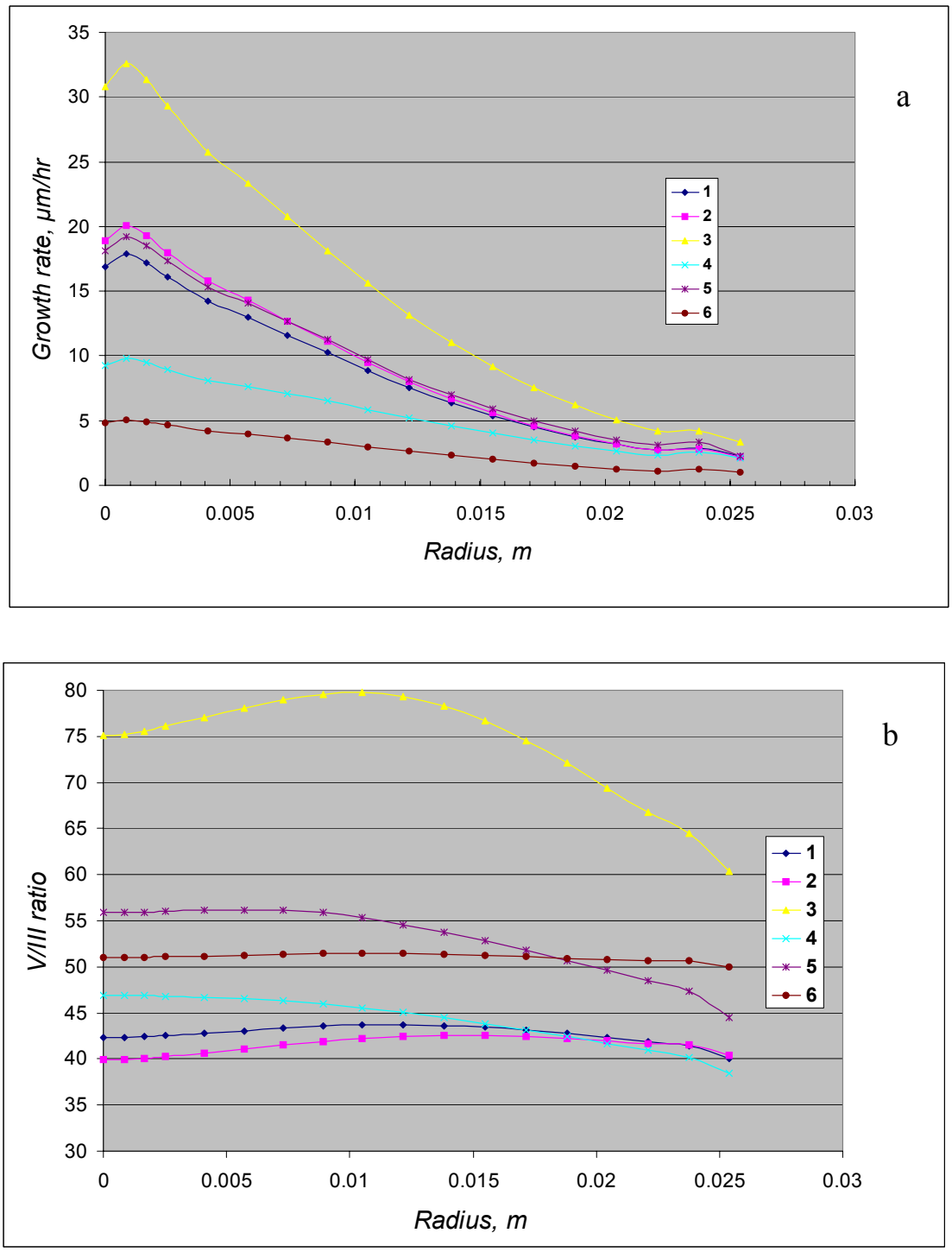

Figure 3. *Radial distributions of the growth rate (a) and V/III ratio (b) at the wafer in the reactor shown in Fig.2 in variation of the characteristic reactor sizes.*

Multi-wafer reactors – simulations and preliminary optimization

With the experience gained in study of the single-wafer reactors, we have turned to multi-wafer reactors. We started with a direct scaling of the previously studied single-wafer reactor with the coaxial species supply. The results of computations have shown, however, that the growth characteristics essentially degrade in this case due to the sharply increasing effects of natural concentration convection. These effects result in generation of a mighty vertical motion above the susceptor, which eventually results in a worse uniformity of the growth rate distributions over the wafers and in a more intensive formation of the parasitic deposit on the reactor walls. Thus, the process optimization is largely reduced in this case to the suppression of natural concentration convection.

After a long series of optimizing computations, we have obtained the desired results, which are illustrated in Figs.5 and 6. In the optimized reactor, the 178 mm diameter susceptor (the other sizes can again be extracted by direct scaling) is rotated at the rate of 60 rpm, the species flow rates are selected as 78 slm of Ar, 40 slm of NH_3, and 2 slm of GaCl. Two original modifications of the reactor design have been additionally introduced here, they are a coaxial hole in the susceptor and a thick coaxial rod above this hole. Positive effect of the hole is related to the reduction of the susceptor area while the rod reduces the total free space in the reactor and orients the flow in the desired direction. Fig. 4a shows that the flow pattern is remarkably uniform in the optimized reactor. No recirculation zone is generated above the susceptor while the precursors are uniformly intermixed (Figs. 4 b and c). The parasitic deposit is distinctly formed on the conic walls of the reactor and coaxial rod, however, its growth rate is much lower than that of the epilayer at the wafer (Fig. 4d). Fig. 5 shows the radial growth rate distributions at the upper susceptor surface in the initial and last (after the optimization) computations. It is seen that the average growth rate is increased from 3 μm/hr to 10.5 μm/hr while the non-uniformity of its distribution (standard deviation from the average value) is reduced from 60% to about 7%.

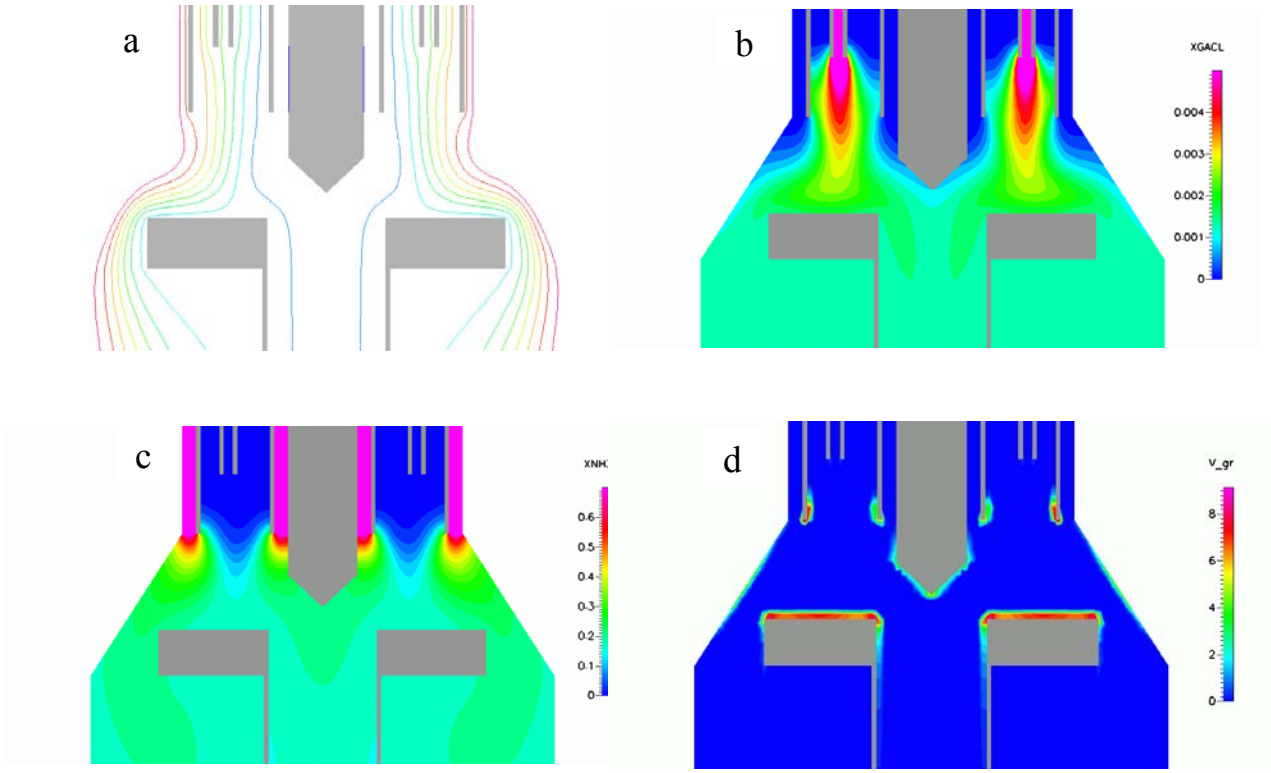

Figure 4. *Streamlines pattern (a), spatial distributions of the GaCl and NH_3 molar fractions (b,c), and surface distributions of the GaN growth rate over different surfaces in the optimized reactor with the species supply through a set of coaxial annular inlets (d).*

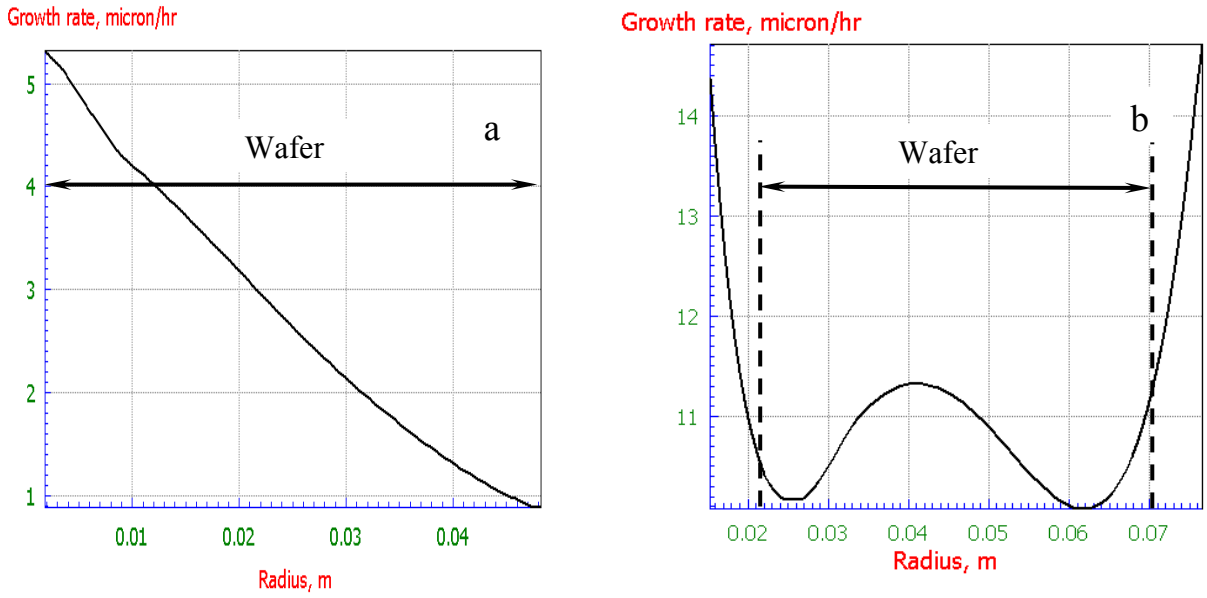

Figure 5. *Radial distributions of the crystal growth rate at the upper susceptor surface in the reactor shown in Fig.2 in the initial (a) and last (b) computation after the optimization.*

Similar to the single-wafer case, the multi-wafer tube reactor with the species supply through a set of separate parallel tubes has exhibited much poorer growth characteristics, and it is not presented here..

Multi-wafer reactors - final optimization

Final optimization of the two selected multi-wafer reactors has been carried out using the mighty computational equipment specially purchased for this aim within the project. The equipment represents a multi-processor computational cluster based on the dual 2 GGz Xeon processors. The optimization involves variation of both the process parameters (temperature, pressure, species flow rates, and susceptor rotation rate) and geometrical sizes of the reactors. To overcome the harmful effect of natural concentration convection, we have suggested at this stage an additional technological solution employing the mixture of 60% H_2 and 40% Ar as the carrier gas. This mixture has the average molar mass close to that of NH_3 and thus provides a low density variation over the system.

Some results of the optimization of III-nitride HVPE in the tube reactor with the species supply through a set of separate parallel tubes are presented in Fig. 6. Here, GaCl and NH_3 are supplied through a set of thin and thick tubes, respectively, while the carrier gas mixture comes into the reactor through an annular slit in the upper part. The streamline pattern (Fig. 6a) in the optimized reactor proves much more uniform compared to the initial case. Simultaneously, the precursors are sufficiently intermixed before they reach the susceptor. Distributions of their molar fractions in several horizontal cross-sections (Fig. 6 b and c) distinctly show that the inlet streams of the gas coming out from the injectors relax above the susceptor. As a result, the crystal growth rate distribution (Fig. 6d) proves rather uniform though the average level of the growth rate is still too low here.

Our attempts to raise the average growth rate in this reactor have not given a successful result. We have tested, in particular, elevation of the susceptor to the injectors and/or increase of the species flow rates. Both the solutions do raise the average growth rate but simultaneously violate the uniformity of its distribution, since the inlet gas streams are not in time to relax until they reach the susceptor. Certain positive effect is provided by increase of the number of the inlet species injectors, however, the reactor design approaches in this case to the alternative solution of the coaxial species supply. Thus, the optimizing computations have suggested once again that the reactor with the species supply through a set of coaxial annular inlets provides better growth characteristics. Finally, we have selected the latter design and performed a careful optimization of III-nitride HVPE in this reactor. The optimization was complicated in this case by the constructional requirement that the side reactor wall would be performed as single cylindrical blocks without any conic parts (unlike the reactor shown in Fig. 4). Besides, the species flow rates should be reduced as much as possible. Despite these restrictions, we managed to achieve the desired combination of the average flow rate, high uniformity of its distribution over the wafer, and low parasitic deposit formation. The results of the final optimization are presented in Figs. 7-9.

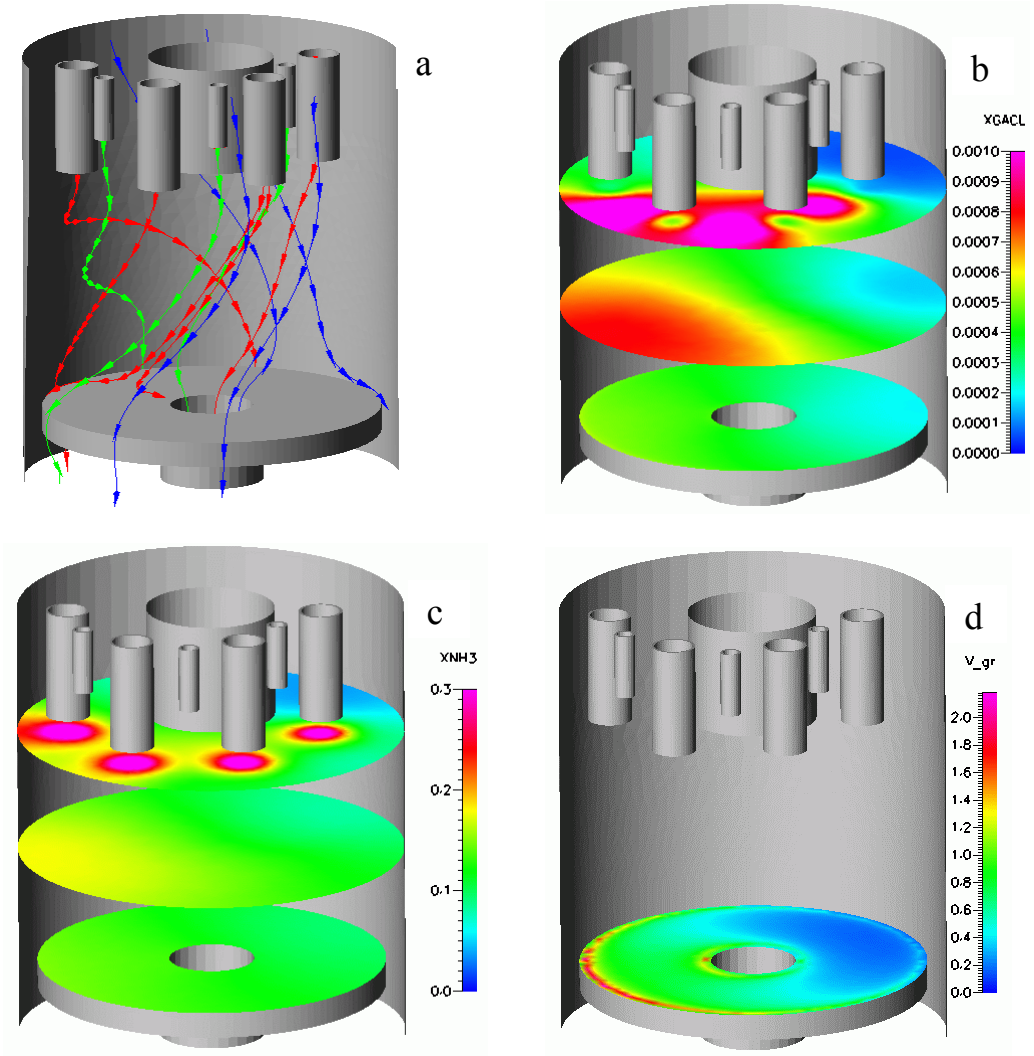

Figure 6. *Streamlines pattern (a), spatial distributions of the GaCl and NH_3 molar fractions (b,c), and surface distribution of the GaN growth rate over the susceptor (d) in the optimized reactor with the species supply through a set of separate parallel tubes.*

Fig. 7 shows the selected reactor sizes and species flow rates. We managed to decrease the species flow rates by several times compared to the previously studied reactor with conic side walls (see Figs. 4,5), where the total GaCl, NH_3, and Ar flow rates were 2, 40, and 78 slm, respectively. The flow pattern and distributions of the species molar fractions in the optimized reactor are shown in Fig. 8. It is seen that the gas flow around the susceptor is remarkably uniform, no vortexes or recirculation zones being generated in the operational zone. Simultaneously, the species are sufficiently well intermixed above the susceptor to provide a uniform growth rate distribution shown in Fig. 9.

To illustrate the optimization procedure, several growth rate distributions corresponding to non-optimal reactor sizes and species flow rates are presented in this figure. It is seen that the growth rate distribution is sensible to the position of the central rod and hole and to the species flow rates. All these parameters should be considered as the main factors controlling the growth rate distribution. The resulting growth rate non-uniformity (standard deviation from the average value) is about 8%, with the average growth rate being of 11.5 μm/hr. Note that the growth rate level obtained may be too high for growth of thin epilayers. However, reducing the inlet concentration of GaCl we will proportionally reduce the average growth rate maintaining its profile over the wafer. Indeed, variation of the low inlet GaCl concentration does not affect the flow dynamics in the system, which is largely determined by NH_3 and carrier gas, but linearly changes the growth rate sensible to the content of the limiting species. The growth rate distribution corresponding to the two times reduced inlet content of GaCl is shown in Fig. 9 by the dashed red line. It is seen that the average growth rate approaches here to the values characteristic for MOCVD but keeps its uniformity.

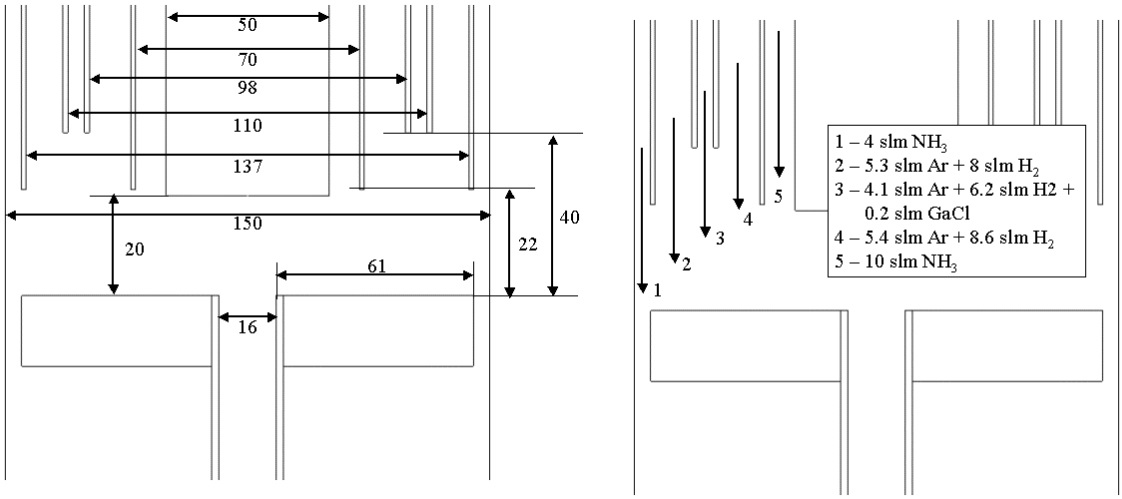

Figure 7. *Selected design, geometrical sizes, and species flow rates providing the optimal growth conditions in the axially symmetric reactor with the species supply through a set of coaxial annular inlets.*

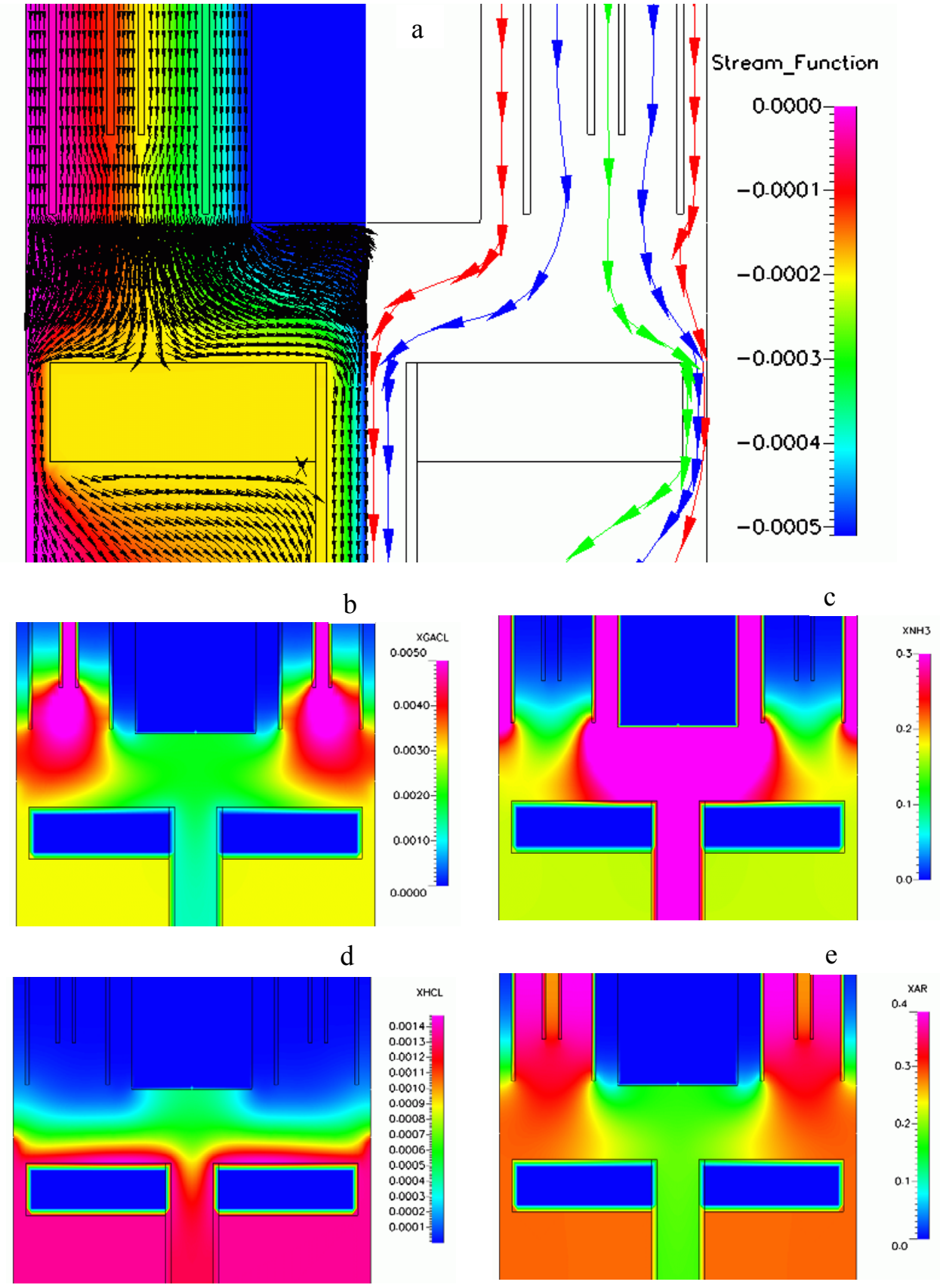

Figure 8. *Flow pattern (a) and species molar fraction distributions (b-e) in the optimized axially symmetric reactor with the species supply through a set of coaxial annular inlets.*

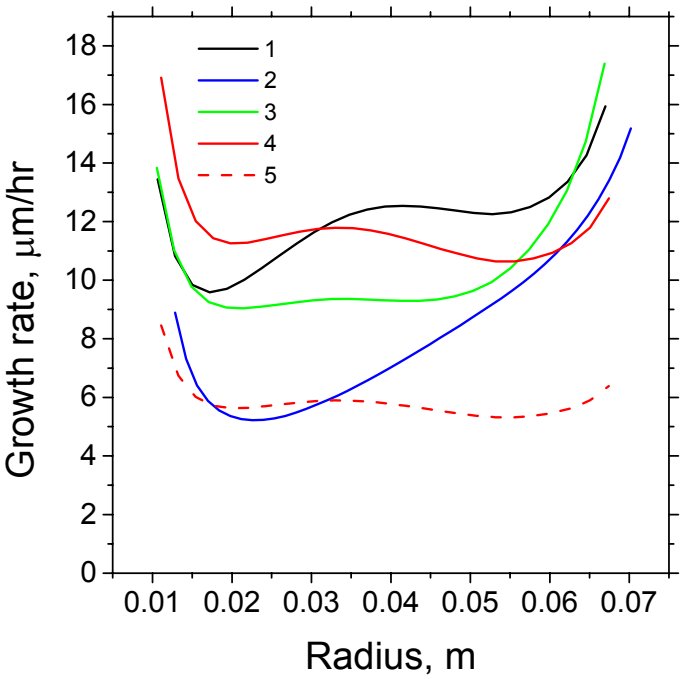

Figure 9. *Radial distributions of the growth rate in axially symmetric reactor with the species supply through a set of coaxial annular inlets: 1 – 5 mm lower central rode, 2 – 2 mm more narrow central hole, 3 – equal inlet velocities through all the annular inlets, 4 – optimized conditions, 5 – optimized conditions with the two times reduced inlet content of GaCl.*

Multi-wafer reactors – transitional effects in change of the species supply

In addition to the above optimization, we have analyzed the transitional effects arising in sharp change of the species supply into the reactor. These effects control variation of the epilayer composition in device structures and thus are of primarily importance for manufacturing of high-quality UVLEDs.

We have considered, in particular, the transitional process arising in sharp "switching-on" or "switching-off" of SiH_4 supply through the annular inlets of the carrier gas in the optimized reactor. Since the two transitional processes are quite similar, we present here only the former process. The results of computations for this case are presented in Figs. 10-12. Fig. 12 shows the instant SiH_4 mass fraction distributions in first 14 seconds after switching-on of the ligand supply. Visually, the distribution seems to stop changing and reach its limit steady state in 10-12 s after the start. This result is confirmed by the corresponding instant radial profiles of the SiH_4 mass fraction shown in Fig. 11. Note that the steady ligand concentration profile proves sufficiently uniform (the standard deviation from the average mass fraction is about 10%). More detailed information on the transitional process is presented in Fig. 12 where relative deviation of SiH_4 mass fraction in the wafer center from its limit steady-state value is presented as a function of time ($\delta(SiH4) = (C_{SiH4}(limit) - C_{SiH4}(t))/(C_{SiH4}(limit) - C_{SiH4}(0))$. It is seen that the ligand concentration approaches to its limit value by three orders of magnitude in about 10 seconds. At the crystal growth rate of about 5 μm/hr (see Fig. 9, red dashed line), this results in 140 A thickness transitional layer.

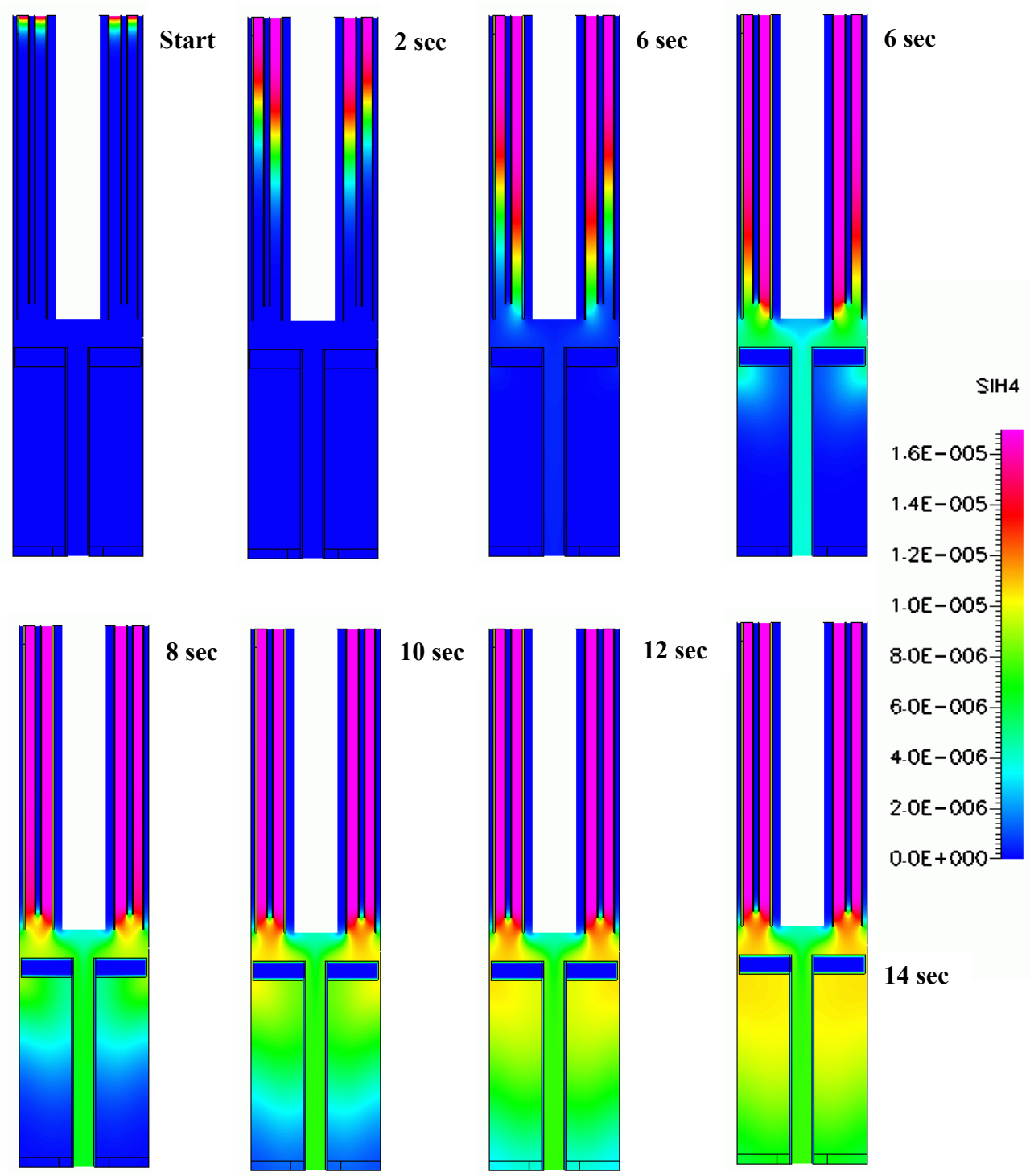

Figure 10. *Successive instant distributions of SiH_4 mass fractions over the optimized reactor for III-nitride HVPE in the first 14 seconds after "switching-on" of the ligand supply.*

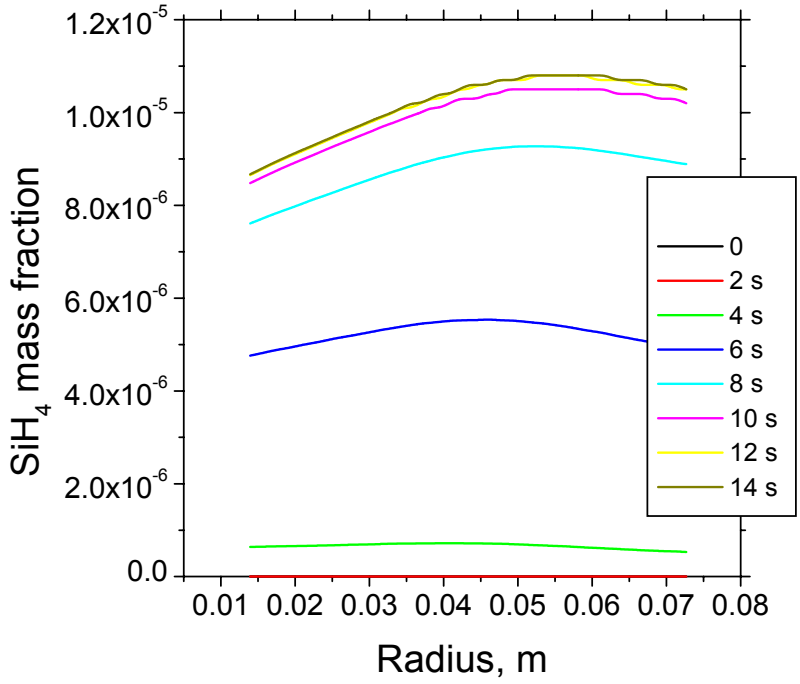

Figure 11. *Successive instant radial profiles of SiH_4 mass fractions over the susceptor in the optimized reactor for III-nitride HVPE in the first 14 seconds after "switching-on" of the ligand supply.*

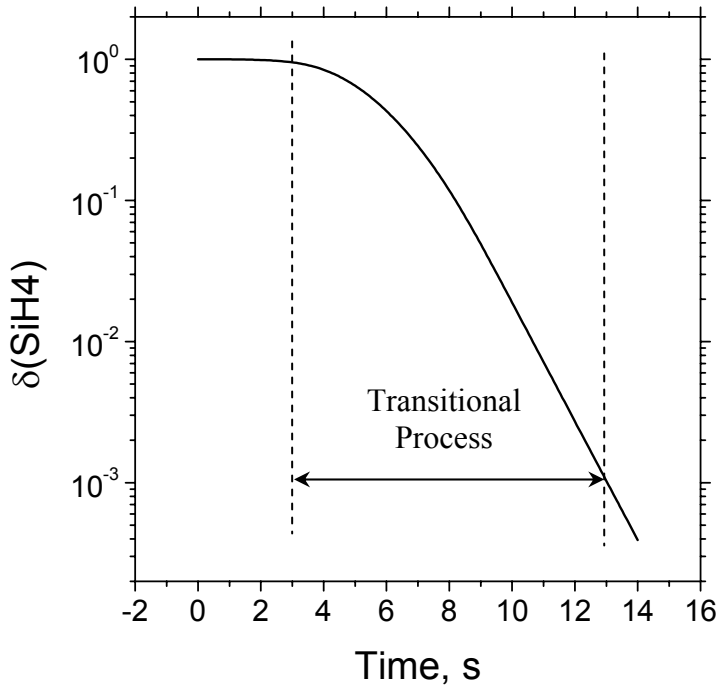

Figure 12. *Relative deviation of SiH_4 mass fraction in the wafer center from its limit steady-state value vs. time.*

Conclusions

Within the project, a predictive model of III-nitride HVPE has been developed and verified using the published experimental data. With this model and mighty multi-processor computational cluster purchased within the project, the process has been carefully simulated and optimized. As a result, a simple axially symmetric reactor design has been developed and all the reactor geometrical sizes and process parameters have been carefully selected. The optimized process provides the average crystal growth rate of about 10 μm/hr with the standard deviation from the average value of about 8%. Additionally, the transitional processes arising in sharp change of the species supply into the reactor have been simulated. It has been shown, in particular, that the ligand concentration reaches its limit steady-state value in about 5 s, which corresponds to about 140 A transitional layer in the heterostructure.

References

1. S.Yu. Karpov, R.A. Talalaev, Yu.N. Makarov, N. Grandjean, J. Massies and B. Damilano, Surface Science, 450 (2000) 191.
2. S.Yu. Karpov, D.V. Zimina, Yu.N. Makarov, B. Beaumont, G. Nataf, P. Gibart, M. Heuken, H. Jurgensen and A. Krishnan, Phys. Stat. Sol. (a) 176 (1999) 439.
3. W.Zhang, T. Reimann, H.R. Alves, M. Heuken, D. Meister, W. Kreigseis, D.M. Hoffmann, J. Christen, A. Krost and B.K. Meyer, J. Cryst. Growth 234 (2002) 616.
4. R.J. Molnar, W. Gotz, L.T. Romano, and N.M. Johnson, J. Cryst. Growth 178 (1997) 147.
5. S.S. Liu and D.A. Stevenson, J. Electrochem. Soc. 125(7) (1978) 1161.
6. M. Kamp, M. Mayer, A Pelzmann and K.J. Ebeling, MRS Internet J. nitride Semicond. 2 (1997) 26.